Interfering with long non-coding RNA *MIR22HG* processing inhibits glioblastoma progression through suppression of Wnt/β-catenin signalling

Mingzhi Han,[1,2] Shuai Wang,[1] Sabrina Fritah,[3] Xu Wang,[1] Wenjing Zhou,[1] Ning Yang,[1] Shilei Ni,[1] Bin Huang,[1] Anjing Chen,[1] Gang Li,[1] Hrvoje Miletic,[2,4] Frits Thorsen,[1,2,5] Rolf Bjerkvig,[2,3,*] Xingang Li[1,*] and Jian Wang[1,2,*]

*These authors contributed equally to this work.

Long non-coding RNAs play critical roles in tumour progression. Through analysis of publicly available genomic datasets, we found that *MIR22HG*, the host gene of microRNAs miR-22-3p and miR-22-5p, is ranked among the most dysregulated long non-coding RNAs in glioblastoma. The main purpose of this work was to determine the impact of *MIR22HG* on glioblastoma growth and invasion and to elucidate its mechanistic function. The *MIR22HG*/miR-22 axis was highly expressed in glioblastoma as well as in glioma stem-like cells compared to normal neural stem cells. In glioblastoma, increased expression of *MIR22HG* is associated with poor prognosis. Through a number of functional studies, we show that *MIR22HG* silencing inhibits the Wnt/β-catenin signalling pathway through loss of miR-22-3p and -5p. This leads to attenuated cell proliferation, invasion and *in vivo* tumour growth. We further show that two genes, *SFRP2* and *PCDH15*, are direct targets of miR-22-3p and -5p and inhibit Wnt signalling in glioblastoma. Finally, based on the 3D structure of the pre-miR-22, we identified a specific small-molecule inhibitor, AC1L6JTK, that inhibits the enzyme Dicer to block processing of pre-miR-22 into mature miR-22. AC1L6JTK treatment caused an inhibition of tumour growth *in vivo*. Our findings show that *MIR22HG* is a critical inducer of the Wnt/β-catenin signalling pathway, and that its targeting may represent a novel therapeutic strategy in glioblastoma patients.

1 Department of Neurosurgery, Qilu Hospital of Shandong University and Institute of Brain and Brain-Inspired Science, Shandong University; Shandong Key Laboratory of Brain Function Remodeling, Jinan, 250012, China
2 NorLux Neuro-Oncology, Department of Biomedicine, University of Bergen, Jonas Lies vei 91, 5009 Bergen, Norway
3 NorLux Neuro-Oncology Laboratory, Department of Oncology, Luxembourg Institute of Health, L-1526 Luxembourg, Luxembourg
4 Department of Pathology, Haukeland University Hospital, 5021 Bergen, Norway
5 The Molecular Imaging Center, Department of Biomedicine, University of Bergen, Jonas Lies vei 91, 5009 Bergen, Norway

Correspondence to: Rolf Bjerkvig
NorLux Neuro-Oncology, Department of Biomedicine, University of Bergen, Jonas Lies vei 91, 5009 Bergen, Norway
E-mail: Rolf.Bjerkvig@uib.no

Correspondence may also be addressed to: Xingang Li
Department of Neurosurgery, Qilu Hospital of Shandong University and Institute of Brain
and Brain-Inspired Science, Shandong University; Shandong Key Laboratory of Brain
Function Remodeling, Jinan, 250012, China
E-mail: Lixg@sdu.edu.cn

Jian Wang
E-mail: Jian.wang@uib.no

Introduction

Non-coding RNAs (ncRNAs), especially long non-coding RNAs (lncRNAs) and microRNAs (miRNAs), have important roles in a wide variety of cellular and physiological functions (Cech and Steitz, 2014; Adams et al., 2017). LncRNAs are defined as transcripts that are >200 nucleotides long without or with limited protein coding potential. LncRNAs exert their functions through a number of mechanisms. They are known to regulate gene expression either in cis (regulate neighbouring genes) or in trans (regulate long-distance genes) in the nucleus (Gupta et al., 2010; Hacisuleyman et al., 2014; Trimarchi et al., 2014). On the other hand, cytoplasmic lncRNAs have been shown to regulate cellular functions through post-transcriptional processing competing with endogenous-RNA (ceRNA) (Yoon et al., 2012; Sahu et al., 2015).

Adding to their roles in normal physiological processes, lncRNAs are novel regulators in oncogenesis, displaying both oncogenic and tumour suppressive effects in many cancers, such as in the breast, prostate, and liver (Gupta et al., 2010; Malik et al., 2014; Yuan et al., 2014). Recent studies also linked several lncRNAs to glioblastoma (GBM) development and pathogenesis (Xi et al., 2018). For instance, the interaction between NEAT1 and the histone-lysine N-methyltransferase enzyme EZH2 mediates histone H3K27 methylation in target promoters, thereby activating the Wnt/β-catenin pathway and thus promotes glioma proliferation and invasion (Chen et al., 2018). The HOTAIR transcript interacts with the polycomb repressive complex 2 (PRC2) and promotes cell cycle progression in GBM (Zhang et al., 2015). Finally, MIR155HG generates miR-155, which enhances proliferative and invasive capacities of glioma cells (Wu et al., 2017). Although a large number of lncRNAs have been identified in GBMs by RNA sequencing (Reon et al., 2016; Paul et al., 2018), their regulatory mechanisms and biological functions are still not fully understood. Thus, studying GBM-associated lncRNAs is important for the discovery of novel prognostic markers and therapeutic targets.

Here, we first performed analysis on publicly available genomic databases and identified the MIR22 host gene (MIR22HG) as a putative molecule involved in glioma tumorigenesis and cancer stem cell function. We subsequently conducted functional analyses of MIR22HG in vitro and in vivo to evaluate its value as a novel molecular therapeutic target. Our results show that MIR22HG promotes glioma progression and self-renewal by producing miR-22-3p and miR-22-5p. Our findings uncover a new mechanism for dysregulation of canonical Wnt/β-catenin signalling, suggesting MIR22HG as a key therapeutic target in GBMs.

Materials and methods

Ethics statement

The research strategy was approved by the Research Ethics Committee of Shandong University and the Ethics Committee of Qilu. All experiments were performed in accordance with relevant guidelines and regulations, and written informed consent was obtained from all patients. Institutional Animal Care and Use Committee (IACUC) of Shandong University approved all surgical interventions and postoperative animal care.

Cell culture

Patient-derived glioblastoma stem-like cells (GSCs) GBM#P3, GBM#BG7, GBM#BG5 and GBM#06 were isolated and functionally characterized from GBM surgical specimens as previously described (Joseph et al., 2014; Fack et al., 2015). These cells were validated by a series of functional assays and express GSC markers such as SOX2 and OLIG2 etc. The DNA fingerprinting of the GSCs was performed by short tandem repeat (STR) profiling (Supplementary Table 1). The human neural stem cells were a kind gift from Prof. Alberto Martínez-Serrano (University of Madrid–CSIC, Spain). Cells were cultured in serum-free Neurobasal™ medium (Gibco/Thermo Fisher Scientific) supplemented with 2% B-27™ Neuro Mix (Thermo Fisher Scientific), 20 ng/ml epidermal growth factor (EGF; Thermo Fisher Scientific), and 10 ng/ml basic fibroblast growth factor (bFGF; PeproTech). Tumourspheres were split using Accutase™ (Thermo Fisher Scientific) to expand GSCs. The U87MG, LN229, and LN18 cell lines were purchased from the Culture Collection of the Chinese Academy of Sciences, and cultured in Dulbecco's modified Eagle medium (Thermo Fisher Scientific) supplemented with 10% foetal bovine serum (FBS; Thermo Fisher Scientific). Normal human astrocytes were obtained from Lonza and cultured in the provided astrocyte growth medium supplemented with rhEGF, insulin, ascorbic acid, GA-1000, L-glutamine and 5% FBS.

Nuclear and cytoplasmic fractionation

Nuclear and cytoplasmic protein fractions were isolated using nuclear and cytoplasmic extraction reagents (Thermo Fisher

Scientific), according to the manufacturer's instructions. Levels of GAPDH and histone H3 were used as loading controls for cytoplasmic and nuclear fractions.

Invasion assays

To assess how *MIR22HG* knockdown affected tumour cell invasion we carried out two invasion assays: a 3D tumour spheroid invasion assay into an invasion matrix and a co-culture assay where GSCs invaded into normal brain organoids. In the matrix assay, GBM#P3 or GBM#BG7 spheres embedded into an invasion matrix (Trevigen). The spheroid at 0 h was used as a reference point for measurement of the distance invaded by sprouting cells.

For the GBM-brain organoid co-culture invasion *ex vivo* system, the preparation and culture of 18-day foetal brain organoids have been described in our previous work (Bjerkvig *et al.*, 1986). After 21 days in culture, the differentiation of cells in normal brain organoids was completed and ready to be confronted with tumour cells. Rainbow barcoded GBM#BG7 cells were established using three lentiviruses (GFP, RFP, CFP). Rainbow-GSCs ($n = 5000$), transfected with small interfering (si)RNAs, were seeded into 96-well plates for 4 days to generate tumour spheroids and then co-cultured with mature brain organoids for 72 h. Confocal microscopy was used to capture images of tumour cell invasion (Leica TCS SP8). ImageJ software (https://imagej.nih.gov/ij/, USA) was used for invasion analysis.

Reporter assay

TOP/Flash reporter plasmids were purchased from GenePharma (http://www.genepharma.com/). The 3′ untranslated region (UTR) of *SFRP2* and *PCDH15*, containing miR-22-3p and miR-22-5p binding sequences, respectively, were cloned into the pmirGLO reporter vectors expressing firefly and *Renilla luciferase*. A mutation in the putative binding sequences in the 3′ UTRs was used as a control. For luciferase-based reporter assays, cells were transfected with the indicated reporter genes and plasmids using Lipofectamine® 3000 (Invitrogen/Thermo Fisher Scientific) according to the manufacturer's instructions. After 48 h, cells were harvested and luciferase activity was determined using a Promega kit (E2920).

Immunofluorescence

Immunofluorescence was performed on paraffin-embedded brain slices. After deparaffinization, slides were incubated with primary antibodies against CD147 (Cell Signaling Technology; dilution 1:200) and subsequently with the appropriate 568-conjugated secondary antibodies (Thermo Fisher Scientific; dilution 1:1000). DAPI (1 µg/ml) was used to visualize nuclei.

In vitro extreme limiting dilution assay

GSCs were placed in a 96-well plate at a density of 1 to 50 cells/well with six replicates for each concentration. After 10 days, the numbers of tumourspheres in each well were

determined, and the sphere formation efficacy was calculated using extreme limiting dilution analysis as previously described (Alvarado *et al.*, 2016; Wang *et al.*, 2018).

Molecular docking-based virtual high-throughput screening

Pre-miR-22 sequences were obtained from the miRBase database (http://microrna.sanger.ac.uk/sequences/). 3D structures of the pre-miR-22 hairpin loop were built using the MC-Fold/MC-Sym pipeline. Openbabel (https://openbabel.org/docs/dev/Installation/install.html) was used to construct the 3D structure of 4786 small molecular compounds provided by the National Cancer Institute (NCI) diversity dataset. The AutoDock program (http://autodock.scripps.edu) was used to perform high throughout molecular dockings for the Dicer enzyme binding site in the hairpin loop of pre-miR-22 against these small molecular compounds.

Animal studies

For intracranial xenograft studies, 4-week-old male athymic nude mice (SLAC laboratory animal Center; Shanghai, China) were bred under specific-pathogen-free conditions at 24°C on a 12-h day-night cycle. For orthotopic transplantation, mice were grouped randomly and were anaesthetized with an intraperitoneal injection of stock solution containing ketamine HCl (25 mg/ml), xylazine (2.5 mg/ml), and 14.25% ethyl alcohol (diluted 1:3 in 0.9% NaCl). U87MG, GBM#P3 or GBM#BG7 cells (10^6 per mouse; five mice per group) were implanted into the right frontal lobes of each mouse by intracranial injection (1 mm anterior, 2.5 mm lateral to the bregma and at a depth of 3.5 mm). Mice were euthanized when neurological symptoms appeared. The mice were then perfused with physiological saline and 4% paraformaldehyde (PFA). The brain of each mouse was harvested, and further fixed in 4% PFA before embedding in paraffin and haematoxylin and eosin staining. For the subcutaneous GBM model, nude mice were divided into two groups (vehicle or AC1L6JTK treatment, five mice per group). GBM#P3 cells were subcutaneously inoculated into the right flanks of nude mice. The tumour tissues were isolated 14 days after injection and tumour volumes and weights were measured from sacrificed mice.

Statistical analysis

Kaplan-Meier survival curves were generated and compared using the log-rank test. The cut-off level was set at the median value of *MIR22HG* expression levels. A two-tailed χ^2 test was used to determine the association between *MIR22HG* expression and clinicopathological characteristics. Pearson correlation was applied to evaluate the linear relationship between gene expression levels. Kolmogorov-Smirnov test was used to assess the normal distribution of data. The one-way ANOVA test or two-tailed *t*-test was used for all other data comparisons using GraphPad Prism 7.0 (LaJolla, CA, USA). Data for each treatment group were represented as a mean ± standard error of the mean (SEM) and compared with other groups for significance by one-way ANOVA followed by Bonferroni's *post hoc* test (multiple comparison tests). All tests

were two-sided, and *P*-values < 0.05 were considered to be statistically significant.

Data availability

The data that support the findings of this study are available from the corresponding author, upon reasonable request. Additional experimental details are provided in the Supplementary material.

Results

MIR22HG is a highly expressed long non-coding RNA in glioblastoma

To identify differentially expressed lncRNAs in human gliomas, we carried out genomic analysis of publicly available gene expression data collected from WHO grade II–IV tumours. The expression profiles of lncRNAs were extracted from The Cancer Genome Atlas (TCGA) RNA-seq data based on their Refseq annotation, and expression values were normalized and Log2 transformed. Through DESeq differential analysis, we uncovered a total of 456 differentially expressed lncRNAs between GBM ($n = 174$) and low-grade glioma (LGG) samples ($n = 511$; 176 of these lncRNAs were upregulated and 279 were downregulated in GBM relative to LGG) (Supplementary Table 3). The heat map in Fig. 1A summarizes the top 100 differential lncRNAs. The *MIR22* host gene emerged as one of the most differentially expressed lncRNAs (*MIR22HG*; $\log_2$ fold-change = 3.43, adjusted $P = 1.40 \times 10^{-41}$) with increased expression among other previously characterized pro-oncogenic lncRNAs in GBM, such as *HOTAIRM1* (Zhang *et al.*, 2013), *CRNDE* (Zheng *et al.*, 2016), *FOXD3-AS1* (Chen *et al.*, 2016), and *NEAT1* (Chen *et al.*, 2018; Zhou *et al.*, 2018). These results were further corroborated using the Chinese Glioma Genome Atlas (CGGA), where *MIR22HG* appeared among the top two highly expressed lncRNAs ($\log_2$ fold-change = 1.88, adjusted $P = 1.01 \times 10^{-13}$) when overlapped with the top 50 candidates from TCGA data (Fig. 1B). As the function of *MIR22HG* has not been investigated in GBM, we decided to focus on this lncRNA in the subsequent analyses. Next, we evaluated, using the TCGA and CGGA cohorts, *MIR22HG* expression level taking into account the 2016 WHO classification of CNS tumours. *MIR22HG* was lower in LGG-Oligo (*IDH*mut, 1p/19q co-deletion), LGG-Astro (*IDH*mut, 1p/19q non-co-deletion) while higher in LGG-*IDH*wt subtype in TCGA (Fig. 1C and Supplementary Fig. 1A). The GBM-*IDH* wild-type subtype, which is associated with worse clinical outcomes, expressed *MIR22HG* at high levels (Fig. 1C and Supplementary Fig. 1A). In addition, data from the Cancer Cell Line Encyclopedia demonstrated that glioma cell lines exhibited higher expression of *MIR22HG* than most other cancer cell lines (Supplementary Fig. 1B). As there are limited

expression data available from human brain tissue, the above comparisons were done between LGGs and GBMs. However, to confirm the increased expression of *MIR22HG* compared to normal brain, we performed *in situ* hybridization on an independent cohort of gliomas ($n = 18$) and normal brain tissue ($n = 5$) from Qilu Hospital. *MIR22HG* was consistently higher expressed in GBM samples compared to LGG ($P < 0.05$) and normal brain tissue ($P < 0.001$) (Fig. 1D and E).

Moreover, *MIR22HG* was found to be preferentially expressed in glioblastoma stem-like cells compared to normal neural stem cells (NSCs) based on microarray data described by Pollard *et al.* (2009) ($P < 0.01$; Fig. 1F) and Liu *et al.* (2014) ($P < 0.001$; Supplementary Fig. 1C). Finally, we interrogated the chromatin landscape of *MIR22HG* in GBM by using the ChIP-seq data derived from GEO and ENCODE databases. We found enrichment of H3K27ac peaks (marker of enhancer) at the promoter region of *MIR22HG* in GBM compared to normal brain tissue, along with an upregulation of *MIR22HG* enhancers in GSC versus differentiated glioma cells (Supplementary Fig. 1D). These results confirm an active *MIR22HG* transcriptional activity in GBM.

In summary, these data show that *MIR22HG* expression is elevated in GBM and could serve as a novel diagnostic marker.

Increased expression of *MIR22HG* is associated with poor survival in glioma patients

Clinicopathological and genetic characteristics have been associated with overall survival in glioma patients. Patient age and genetic features, including O-6-methylguanine-DNA methyltransferase (*MGMT*) promotor methylation, codeletion of 1p/19q, telomerase reverse transcriptase (*TERT*) loss, and *IDH* (CeccarelLi *et al.*, 2016; Louis *et al.*, 2016) and ATRX chromatin remodeler (*ATRX*) mutations, have been reported to be associated with a favourable prognosis (Yan *et al.*, 2009; Jiang *et al.*, 2016; Louis *et al.*, 2016). We therefore analysed whether high or low expression of *MIR22HG* correlated with any of these characteristics. High expression of *MIR22HG* was statistically associated with patient age ($\geqslant 45$ years; $P < 0.001$) and Karnofsky Performance Score (< 80; $P < 0.001$), but did not correlate with gender ($P = 0.913$; Supplementary Table 4). Low *MIR22HG* was found to be associated with methylated *MGMT*, 1p/19q codeletion, loss of *TERT* and mutated *ATRX* in tumours ($P < 0.001$; Supplementary Table 4).

Kaplan-Meier analysis was performed to examine the relationship between patient survival and *MIR22HG* expression. Over 1500 cases were enrolled from three independent databases that were then assigned an *MIR22HG*^{high} or *MIR22HG*^{low} expression status determined by the median expression levels. The *MIR22HG*^{high}
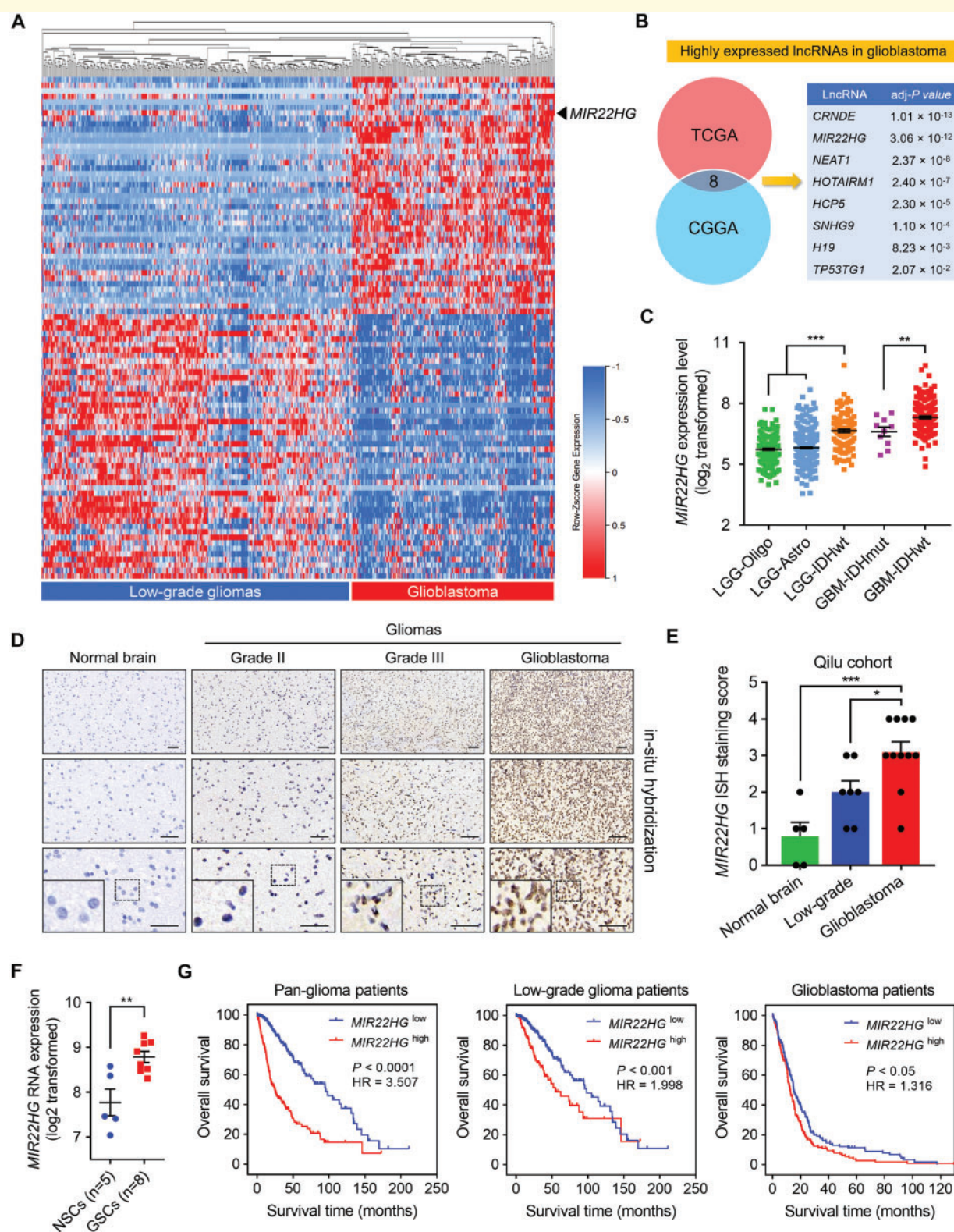
Figure 1 *MIR22HG* expression is elevated in GBM. (**A**) Heat map of the top 100 differentially expressed lncRNAs between LGG and GBM from TCGA dataset; gene expression values are z-transformed and are coloured red for high expression and blue for low expression; red arrow indicates *MIR22HG*. (**B**) Venn plot displaying the significantly upregulated lncRNAs in GBM in both TCGA (top 50 upregulated lncRNAs) and CGGA (top 50 upregulated lncRNAs). (**C**) *MIR22HG* RNA expression (log2) based on 2016 WHO classification from TCGA. (**D**) Representative images of RNA *in situ* hybridization staining for *MIR22HG* in normal brain (*n* = 5) and different pathological grades of gliomas (*n* = 18). Scale bar = 100 μm. (**E**) Graphic representation of the quantification of *MIR22HG in situ* hybridization staining in normal brain and different pathological grades of gliomas. (**F**) *MIR22HG* RNA expression (log2) in NSCs and GSCs from GSE15209. (**G**) Kaplan-Meier analysis of patient overall survival data based on high versus low expression of *MIR22HG* in gliomas, grades II–IV, from the TCGA dataset. *P*-values were obtained from the log-rank test. Data are shown as mean ± the standard error of the mean (SEM) for each group. *P < 0.05, **P < 0.01, ***P < 0.001.

group patients exhibited significantly shorter overall survival as well as progression-free survival compared to the *MIR22HG*^{low} group in all cohorts (Fig. 1G and Supplementary Fig. 1E–G). In addition, *MIR22HG* levels significantly associated with poor survival in cases with wild-type *IDH* (Supplementary Fig. 1H). Finally, *MIR22HG* was validated as an independent prognostic indicator in univariate and multivariate Cox regression analysis of overall survival [hazard ratio (HR) = 1.177, 95% confidence interval (CI) = 1.034 to 1.339, $P = 0.009$; Supplementary Table 5] and progression-free survival (HR = 1.617, 95% CI = 1.617 to 2.499, $P = 0.030$; Supplementary Table 6) in glioma patients.

Silencing *MIR22HG* inhibits glioblastoma malignant phenotypes and GSC maintenance

To predict the *MIR22HG*-associated biological functions in gliomas, we performed Gene Set Enrichment Analysis (GSEA) using the TCGA GBM dataset. Biological processes, including proliferation, apoptosis, stem cell function, and tumour invasion exhibited the strongest association with high *MIR22HG* levels (Fig. 2A).

We first detected the expression levels of *MIR22HG* in a panel of GBM cell lines including three GBM cell lines (U87MG, LN229, LN18) and four patient-derived primary GSCs (GBM#P3, GBM#BG7, GBM#BG5 and GBM#06). In addition, two non-cancer cell lines, human NSCs, and normal human astrocytes were also included as normal controls. At the expression level, both human NSCs and normal human astrocytes displayed lower *MIR22HG* expression levels compared to all GBM cells by quantitative reverse-transcription PCR (qRT-PCR) (Fig. 2B). Similar results were observed based on microarray data where multiple GBM cell lines possess higher expression than human NSCs (Supplementary Fig. 2A). Between the GBM cells, U87MG and GBM#P3 displayed the highest *MIR22HG* expression among all cell lines (Fig. 2B).

To determine its biological function, *MIR22HG* was targeted in seven GBM cell lines (three cell lines and four patient-derived primary GSCs) and two normal controls (normal human astrocytes and human NSC) by using two independent siRNAs compared to a control non-targeted-siRNA (si-Ctrl) (Supplementary Fig. 2B). We validated the *MIR22HG* knockdown efficacy by qRT-PCR (Fig. 2C and Supplementary Fig. 2C). Targeting *MIR22HG* potently impaired proliferation in GBM cell lines and GSCs derived from multiple patients ($P < 0.01$, respectively; Fig. 2D). In contrast, targeting *MIR22HG* minimally reduced cell proliferation in human NSCs and normal human astrocytes.

Flow cytometry apoptosis assays showed that inhibition of cell growth was mediated both by an increased apoptotic cell death ($\sim$2-fold compared to controls in U87MG, GBM#P3 and GBM#BG7) (Fig. 2E and Supplementary

Fig. 2D) and an induction of cell cycle arrest in the G0/G1 phase (Supplementary Fig. 2E). An increase in proteins involved in these biological processes, including the apoptotic indicator cleaved-PARP and cell cycle arrest markers such as p21 and p27, were correspondingly induced (Fig. 2F).

Given that *MIR22HG* was highly expressed in GSCs compared to NSCs (Fig. 1F and Supplementary Fig. 1C), we determined the impact of *MIR22HG* knockdown on stem cell-associated properties. In tumoursphere formation and extreme limiting dilution assays (ELDA), *MIR22HG* knockdown resulted in a remarkable decrease in sphere formation in GBM#P3, GBM#BG7, GBM#BG5 and GBM#06 cells (Fig. 2G, H and Supplementary Fig. 2F and G).

MIR22HG knockdown inhibits tumour invasion and growth *in vivo*

Next, we examined the influence of *MIR22HG* knockdown on glioma cell invasion. Analysis of intra-tumoural transcriptional heterogeneity based on the IVY project (http://glioblastoma.alleninstitute.org/) (Puchalski *et al.*, 2018) demonstrated that *MIR22HG* was expressed higher in the infiltrating region of tumours compared to the tumour core (Supplementary Fig. 3A and B). In a 3D spheroid invasion assay, knockdown of *MIR22HG* attenuated the invaded distance of GBM#P3 cells by $\sim$50% ($P < 0.01$; Fig. 3A). To confirm these results, we also established a novel co-culture invasion model where brain organoids were co-cultured with GBM spheroids based on our previous work (Bjerkvig *et al.*, 1986), thus mimicking the physiologically invasive brain microenvironment of glioma cells (Fig. 3B). Using this *ex vivo* model, rainbow-si-Ctrl or -si-*MIR22HG* cells were cultured for 4 days to generate tumour aggregates and then co-cultured with mature rat brain organoids. After 72 h, the number of cells invading the brain organoids as well as the area invaded by tumour cells was significantly decreased in the si-*MIR22HG* group compared to the si-Ctrl group in both GBM#BG7 ($P < 0.05$; Fig. 3C and D) and GBM#P3 cells ($P < 0.001$; Supplementary Fig. 3D).

To validate our *in vitro* observations, tumour growth was assessed in orthotopic xenograft models (U87MG, GBM#P3 and GBM#BG7) transduced with a lentivirus expressing sh-Ctrl ($n = 5$) or sh-*MIR22HG* ($n = 5$). Knockdown of *MIR22HG* significantly reduced tumour growth and prolonged overall survival of tumour-bearing mice ($P < 0.001$, $P < 0.05$ and $P < 0.05$, respectively) (Fig. 3E, F and Supplementary Fig. 4A–C). The proliferation index marker Ki-67 was decreased in sh-*MIR22HG* xenografts (Fig. 3G and Supplementary Fig. 4D), and importantly, these tumours displayed more circumscribed borders relative to the sh-Ctrl xenografts (Fig. 3F). Immunofluorescence staining for a human specific antigen (CD147) revealed a decrease in satellite lesions and invasive
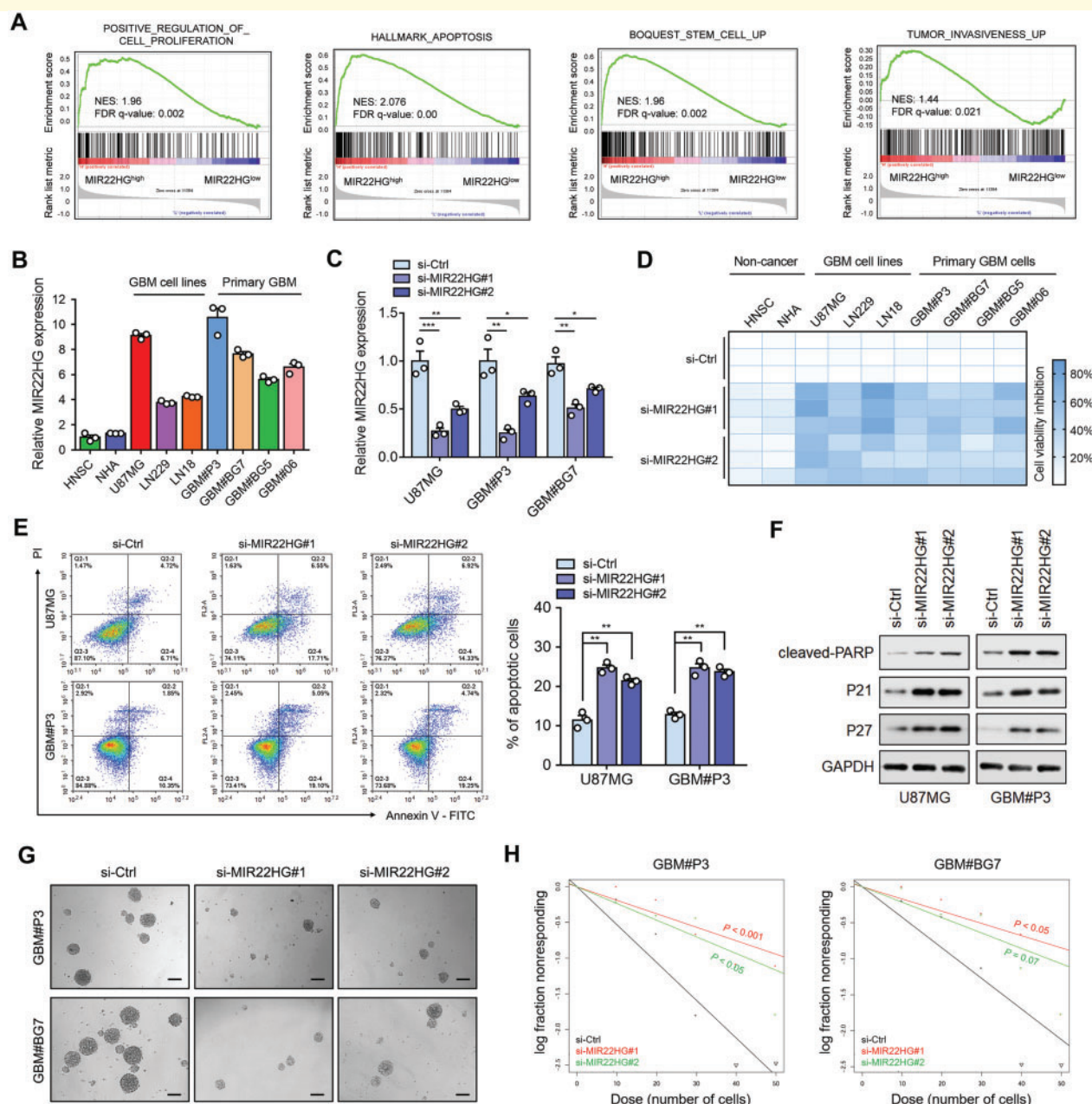
Figure 2 *MIR22HG* promotes cell growth and self-renewal in GBM. (**A**) GSEA highlighting positive association of *MIR22HG*^{high} co-regulated genes with cell proliferation, apoptosis, stem cell regulation, and invasion gene signatures. FDR = false discovery rate; NES = normalized enrichment score. (**B**) qRT-PCR analysis of *MIR22HG* RNA expression in two non-cancer cell lines and seven GBM cell lines. *GAPDH* was used for normalization. (**C**) qRT-PCR analysis of *MIR22HG* RNA expression in U87MG, GBM#P3 and GBM#BG7 cells after transfection with si-Ctrl or two different siRNAs (si-MIR22HG#1 and si-MIR22HG#2) for 48 h (*n* = 3 per group). *GAPDH* was used for normalization. (**D**) Heat map represents the cell viability inhibition of two non-cancer cell lines and seven GBM cell lines transfected with si-Ctrl, si-MIR22HG#1 or si-MIR22HG#2 (*n* = 3 per group). Cell viability data were obtained from CCK-8 assay and normalized with si-Ctrl group. (**E**) Annexin V-FITC and propidium iodide (PI) staining to assess apoptosis and DNA content using flow cytometry in U87MG and GBM#P3 after transfection with si-Ctrl, si-MIR22HG#1 or si-MIR22HG#2. (**F**) Western blot to detect expression levels of cleaved-PARP, p21 and p27 proteins in U87MG and GBM#P3 after transfection with si-Ctrl, si-MIR22HG#1 or si-MIR22HG#2. (**G**) Representative images from tumoursphere formation assays for GBM#P3 and GBM#BG7 GSCs transfected with si-Ctrl, si-MIR22HG#1 or si-MIR22HG#2. Scale bar = 100 μm. (**H**) Extreme limiting dilution assay performed with GBM#P3 and GBM#BG7 GSCs. Data are shown as mean ± SEM. *$P < 0.05$, **$P < 0.01$, ***$P < 0.001$.

tumour cells in peritumoural areas (Fig. 3H and Supplementary Fig. 4E). Finally, several classical invasive markers, including ZEB1, MMP2 and MMP7, were found to be dramatically decreased in U87MG-sh-MIR22HG xenografts (Supplementary Fig. 4F); while only ZEB1 and MMP2 decreased in GBM#P3 xenografts,
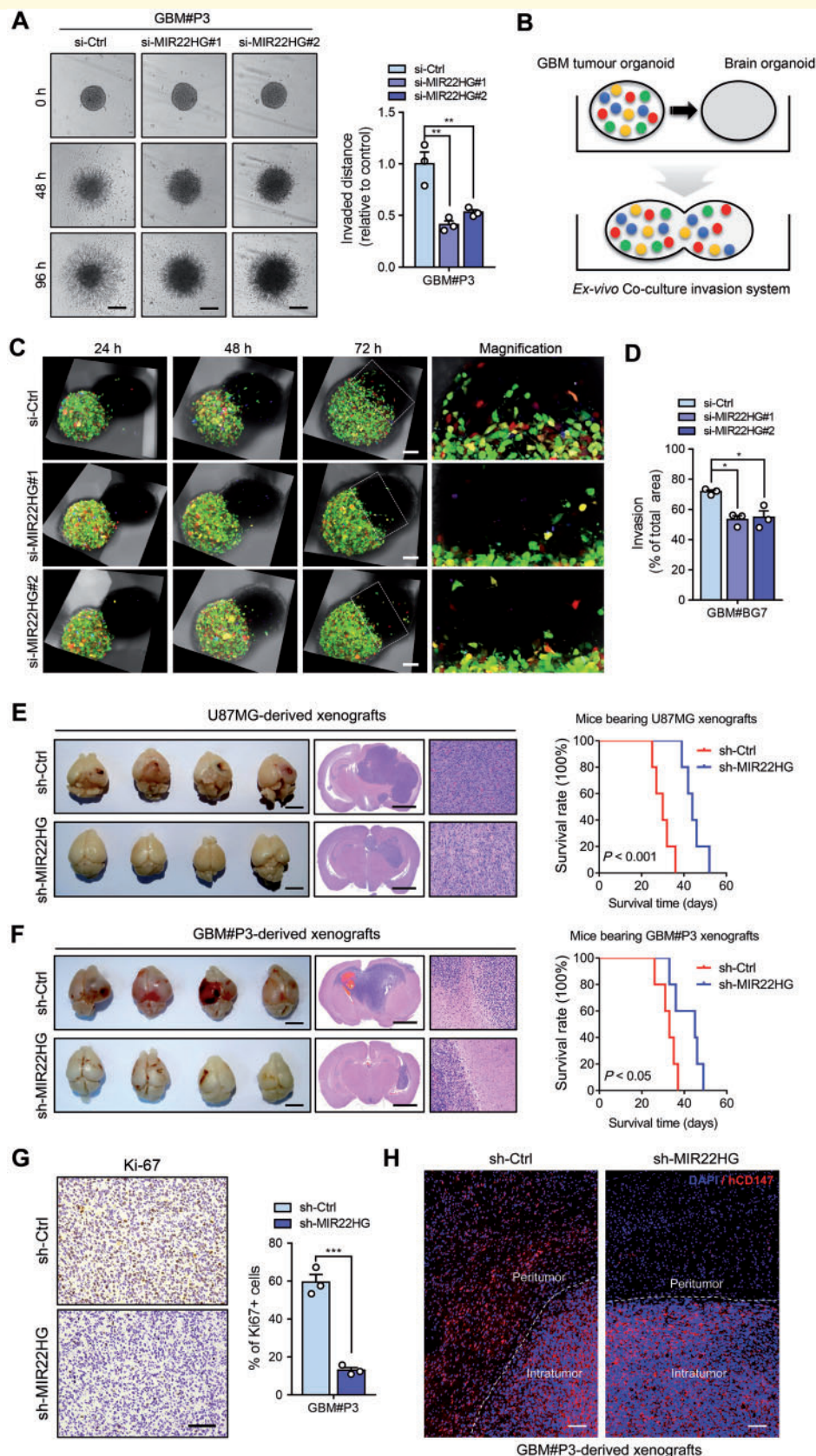
Figure 3 *MIR22HG* **knockdown decreases invasive ability of GBM cells and impairs tumour growth and invasion *in vivo*.**
(**A**) Representative images of spheroids in 3D invasion assays for GBM#P3 GSCs transfected with si-Ctrl, si-MIR22HG#1 or si-MIR22HG#2, and evaluated at 0, 48 and 96 h. Scale bar = 200 μm. Graphic representation of the quantification of the distance of invading cells from the tumourspheres determined after 96 h (*right*). (**B** and **C**) Representative images of co-culture invasion assays for GBM#GB7 GSCs transfected with

(continued)

which might be due to the lower basal expression of MMP7 in GBM#P3 cells (Supplementary Fig. 4F).

In summary, these results support a key role of *MIR22HG* in promoting tumour invasive growth *in vivo*.

MIR22HG modulates the Wnt/β-catenin pathway in glioblastomas

To investigate the potential mechanisms of *MIR22HG* action, genome-wide transcriptomic correlation analysis was performed using the TCGA GBM data (Fig. 4A), where the genes associated with *MIR22HG* (Pearson analysis, $P < 0.01$) were subjected to GO and KEGG analysis. The results revealed *MIR22HG* to be significantly associated with the Wnt signalling pathway (adjusted $P < 0.05$; Fig. 4B). Knockdown studies were performed in U87MG and GBM#P3 cells *in vitro* to determine whether *MIR22HG* was involved in the regulation of the canonical Wnt/β-catenin pathway. *MIR22HG* silencing led to a downregulation of β-catenin, a key transcriptional regulator of Wnt, along with the suppression of several Wnt downstream targets, including c-Myc, cyclin D1, and LEF1 (Fig. 4C). Western blot analysis also revealed an increase in phospho-β-catenin levels, which represents the inactive form of β-catenin (Li *et al.*, 2012). Moreover, a decrease in phospho-GSK3β (Ser9) levels was observed indicating Wnt/β-catenin pathway inactivation (Hui *et al.*, 2018) (Fig. 4C). In addition, knockdown of *MIR22HG* using a TOP/FOP luciferase reporter assay also revealed changes in β-catenin dependent transcriptional activity in U87MG and GBM#P3 cells ($P < 0.05$; Fig. 4D and E). After *MIR22HG* knockdown, levels of both cytoplasmic and nuclear β-catenin were reduced (Fig. 4F and G).

In summary, these data show that alterations in *MIR22HG* levels substantially affects β-catenin protein levels and Wnt signalling activity.

miR-22-3p and miR-22-5p mediate *MIR22HG*-induced glioblastoma progression

MIR22HG has previously been demonstrated to be a host gene of miR-22 (Fig. 5A) (Wang *et al.*, 2012). Given the fact that a major function of certain lncRNAs is the production of embedded miRNAs, we asked if *MIR22HG*-induced glioma progression was mediated by miR-22-3p and miR-22-5p. In culture, we observed, by qRT-PCR, a corresponding decrease of miR-22-3p and miR-22-5p, in U87MG and GBM#P3 *MIR22HG* depleted cells ($>80\%$; $P < 0.01$; Fig. 5B). Meanwhile, based on TCGA data, miR-22 was significantly associated with *MIR22HG* expression status in both LGG (Pearson = 0.4903, $P < 0.001$) and GBM samples (Pearson = 0.4399, $P < 0.001$; Supplementary Fig. 5A). Moreover, miR-22-3p and -5p expression was found to be strongly associated with *MIR22HG* expression ($P < 0.001$; Supplementary Fig. 5B).

In primary tumour samples, both miR-22-3p and -5p were highly expressed in high grade gliomas ($P < 0.001$, respectively; Supplementary Fig. 5C). Moreover, survival analysis demonstrated that higher expression levels of miR-22-3p and -5p were associated with poor overall survival and progression-free survival in glioma patients (Supplementary Fig. 6A–D and Supplementary Tables 7–10). GO analysis using the GBM expression profiles revealed an enrichment of miR-22-3p and -5p negatively-associated genes in the canonical Wnt pathway (Supplementary Fig. 7A). U87MG and GBM#P3 cells were then transfected with miR-22 mimics or anti-miR-22, and overexpression as well as knockdown were confirmed by qRT-PCR (Supplementary Fig. 7B). In functional studies, knockdown of miR-22-3p or -5p resulted in an inhibition of tumoursphere formation ($P < 0.01$ and $P < 0.05$; Supplementary Fig. 7C) and cell invasion capacity ($P < 0.01$ and $P < 0.05$; Supplementary Fig. 7D), along with an induction of apoptosis (Supplementary Fig. 7E) and cell cycle arrest at G0/G1 phase (Supplementary Fig. 7F). These data substantiate oncogenic roles of miR-22s in GBM progression.

To examine whether overexpression of the miR-22s are sufficient to overcome the depletion of their host gene, we transfected miR-22-3p and -5p mimics into U87MG-, GBM#P3- and GBM#BG7-si-*MIR22HG* cells. Ectopic expression of the two miR-22s partially restored tumour cell proliferation (Fig. 5C and Supplementary Fig. 8A and B), but inhibited apoptosis (Fig. 5D and Supplementary Fig. 8C) and cell cycle arrest (Supplementary Fig. 8D); however, miR-22-5p mimics did not significantly reverse cell cycle arrest in U87MG-si-*MIR22HG* cells (Supplementary Fig. 8D), which might be due to the cellular heterogeneity between primary GSCs and adherent serum-culture cell lines. Moreover, cell invasion (Fig. 5E and Supplementary

Figure 3 Continued
si-Ctrl, si-MIR22HG#1 or si-MIR22HG#2, and evaluated at 24, 48 and 72 h. (**D**) Quantification of invading area determined using percentage of area invaded after 72 h. (**E** and **F**) Representative gross images and haematoxylin and eosin staining of mouse brains implanted with U87MG or GBM#P3 cells transduced with sh-Ctrl ($n = 5$) or sh-MIR22HG#1 ($n = 5$), and Kaplan-Meier analysis of corresponding tumour-bearing animals. Scale bar = 2 mm. *P*-values were obtained from the log-rank test. (**G**) Immunohistochemistry for Ki-67 in sections from GBM#P3 xenografts and graphic representation of quantification. Scale bar = 100 μm. (**H**) Immunofluorescence staining for human specific antigen (CD147) in sections of xenografts from GBM#P3 transduced with sh-Ctrl or sh-MIR22HG#1 ($n = 5$). Intratumoural and peritumoural areas are designated to highlight satellite lesions and invasive tumour cells. Scale bar = 100 μm. Data are shown as mean ± SEM. *$P < 0.05$, **$P < 0.01$, ***$P < 0.001$.
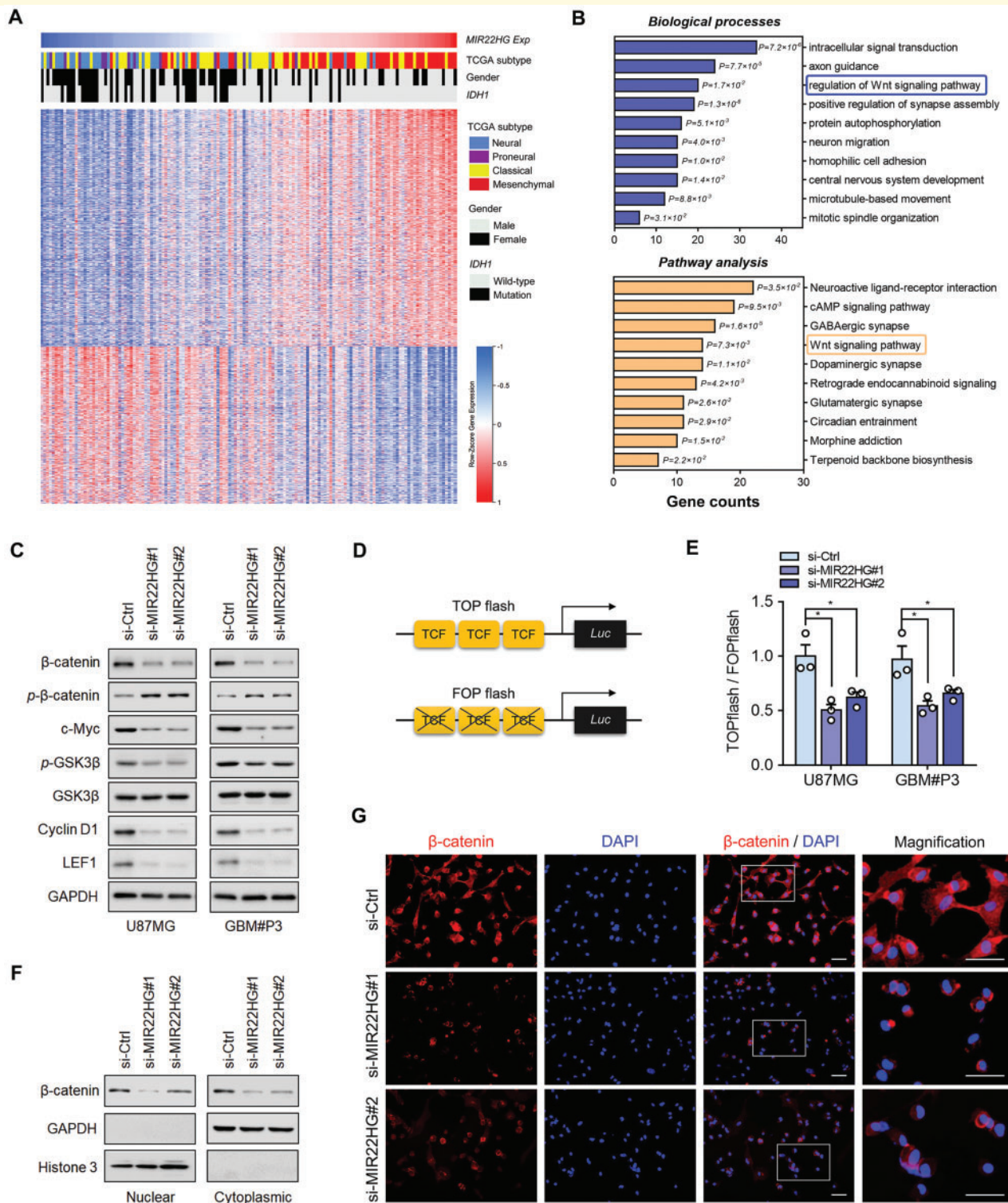
Figure 4 *MIR22HG* activates the Wnt/β-catenin pathway in gliomas. (**A**) Whole-transcriptome hierarchical cluster analysis was performed on *MIR22HG*-associated genes based on *MIR22HG* expression from TCGA GBM data. The resultant heat map shows relative expression levels of *MIR22HG*-associated genes in individual GBM cases where red is higher expression and blue is lower expression. (**B**) Biological processes and pathway analysis performed using the set of *MIR22HG*-associated genes. Results are based on GO and KEGG databases with adjusted *P*-values. (**C**) Western blot for protein levels of Wnt/β-catenin indicators in U87MG and GBM#P3 cells at 48 h after transfection with si-Ctrl, si-MIR22HG#1 or si-MIR22HG#2. GAPDH was used as a loading control. (**D**) Schematic representation of the TOP-Luc and TCF site mutant reporter (FOP-Luc) construct to assess β-catenin activity. (**E**) Graphic representation of relative levels of TOP flash/FOP flash luciferase activity in U87MG and GBM#P3 cells 48 h after transfection with si-Ctrl, si-MIR22HG#1 or si-MIR22HG#2. (**F**) Western blot for levels of β-catenin in cytoplasmic and nuclear lysates prepared from U87MG 48 h after transfection with si-Ctrl, si-MIR22HG#1 or si-MIR22HG#2.
(**G**) Immunofluorescence images for β-catenin (red) and nuclear (blue) staining in U87MG at 48 h after transfection with si-Ctrl, si-MIR22HG#1 or si-MIR22HG#2. Scale bar = 30 μm. Data are shown as mean ± SEM. $^{*}P < 0.05$, $^{**}P < 0.01$, $^{***}P < 0.001$.
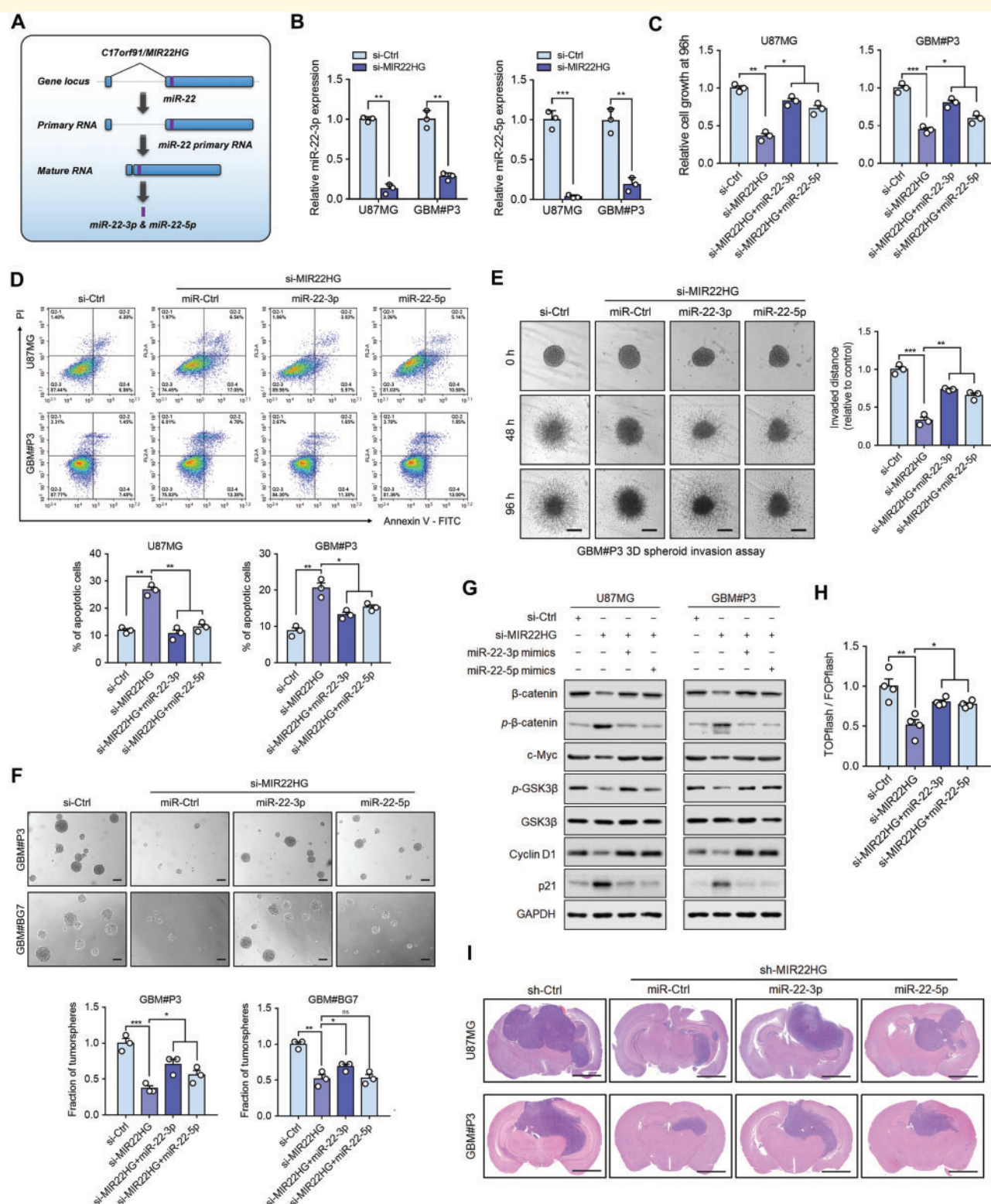
Figure 5 miR-22-3p and miR-22-5p mediate *MIR22HG*-induced GBM progression. (**A**) Schematic model of miR-22 maturation process. (**B**) qRT-PCR analysis of miR-22-3p and -5p expression in U87MG and GBM#P3 cells after transfection with si-Ctrl or si-MIR22HG. (**C**) Relative cell growth for rescue experiments as determined using OD values from the CCK-8 assay at 96 h in U87MG and GBM#P3 cells transfected with si-Ctrl, siMIR22HG + miR-Ctrl, siMIR22HG + miR-22-3p, or siMIR22HG + miR-22-5p. (**D**) Annexin V-FITC and PI staining to assess apoptosis and DNA content using flow cytometry in U87MG and GBM#P3 cells transfected with si-Ctrl, si-MIR22HG, siMIR22HG + miR-22-3p, or siMIR22HG + miR-22-5p. (**E**) Representative images of 3D invasion assay and quantification in miR rescue experiments. GBM#P3 GSCs were transfected with si-Ctrl, siMIR22HG + miR-Ctrl, siMIR22HG + miR-22-3p, or siMIR22HG + miR-22-5p, allowed to form spheres, embedded in the invasion matrix, and evaluated thereafter at the hours indicated. Scale bar = 200 μm. (**F**) Representative images from

Fig. 8E) and tumoursphere formation (Fig. 5F) were correspondingly restored in si-*MIR22HG* cells transfected with miR-22-3p or miR-22-5p (less rescue effect of -5p was observed in GBM#BG7 possibly caused by interpatient cellular heterogeneity). Western blot analysis and the TOP/FOP luciferase reporter assay (U87MG) showed that the introduction of miR-22-3p and -5p mimics into U87MG- and GBM#P3-si-*MIR22HG* cells reversed suppression and activated Wnt signalling (Fig. 5G and H). Immunofluorescence confirmed the restoration of β-catenin expression in U87MG-si-*MIR22HG* (Supplementary Fig. 8F). U87MG cells transduced with lenti-sh-*MIR22HG* and lenti-miR-22-3p or -5p, -partially restored tumour growth and reduced overall survival of tumour-bearing mice compared to the U87-sh-*MIR22HG* group ($P < 0.01$ and $P < 0.05$, respectively) (Fig. 5I and Supplementary Fig. 8G). These results were further validated in GBM#P3-derived xenografts (Fig. 5I and Supplementary Fig. 8G).

Finally, to confirm that *MIR22HG* functions as the host gene of miR-22s in GBM progression and to exclude the effect of the other regions of the full-length 2.6 kb *MIR22HG* transcript, we performed ectopic expression experiments with a *MIR22HG* full-length construct (wild-type, WT), as well as a *MIR22HG* mutant construct, *MIR22HG*-Δexon2 (deletion of miR-22 region in exon 2) (Supplementary Fig. 8H). In a functional assay, we found that overexpression (OE) of *MIR22HG*-WT significantly promoted U87MG cell growth *in vitro* compared to the control group and *MIR22HG*-Δexon2-OE group ($P < 0.001$); while *MIR22HG*-Δexon2-OE minimally promoted cell proliferation in GBM. These data strongly support an oncogenic role of *MIR22HG* as a precursor of miR-22s in GBM.

Taken together, we demonstrate that miR-22s are indispensable in *MIR22HG*-induced GBM growth.

SFRP2 and PCDH15 are downstream targets of miR-22-3p and -5p

We then sought to identify genes that might be directly targeted by miR-22-3p or -5p. Using computational target prediction based algorithms (TargetScan v7.1 and miRanda), several genes were found to have 3′ UTR putative binding sites for miR-22-3p and miR-22-5p (Fig. 6A). Among them, *SFRP2* was further identified to be strongly

negatively associated with miR-22-3p ($Pearson_{miR-22-3p}$ = –0.479, $P < 0.001$; Fig. 6B); a similar relationship was revealed between miR-22-5p and *PCDH15* ($Pearson_{miR-22-5p}$ = –0.351, $P < 0.001$; Fig. 6C). However, other candidates such as TET2 ($Pearson_{miR-22-3p}$ = –0.201), CLIC4 ($Pearson_{miR-22-3p}$ = 0.163), DUSP1 ($Pearson_{miR-22-5p}$ = –0.096) or TXN2 ($Pearson_{miR-22-5p}$ = –0.101), showed no significant UTR association with the miR-22s in gliomas. Therefore, we identified *SFRP2* and *PCDH15* as the most attractive candidates.

The clinical relevance of SFRP2 and PCDH15 was also verified by the TCGA dataset where a lower expression of *SFRP2* and *PCDH15* was associated with a shorter overall survival and progression-free survival in patients ($P < 0.001$; Supplementary Fig. 9A and Supplementary Tables 11 and 12). In addition, the combined expression levels of the miR-22-3p^{high} and SFRP2^{low}, or miR-22-5p^{high} and PCDH15^{low}, in glioma patients, more accurately predicted a shorter overall survival and progression-free survival (Supplementary Fig. 9B). These results were further validated in TCGA GBM patients (Supplementary Fig. 9C).

Secreted frizzled-related proteins (SFRPs) and protocadherins have been shown to be critical for the regulation of canonical Wnt signalling (Lee *et al.*, 2016; Mah and Weiner, 2017). Consistently, GSEA analysis of TCGA data indicated that both SFRP2 and PCDH15 enrichment was associated with Wnt signalling regulation (Supplementary Fig. 10A and B). SFRPs have been shown to have tumour suppressor functions in cancers such as medulloblastoma. By immunohistochemistry staining, the expression of both SFRP2 and PCDH15 was found to be highly expressed in the normal brain and LGG, but to a lesser extent in GBMs (Supplementary Fig. 10C). In addition, these genes were found to be preferentially expressed in non-GSCs ($n = 3$) compared to GSCs ($n = 3$) based on GSE41032 (Supplementary Fig. 10D).

We therefore assessed if miR-22-3p and -5p could regulate *SFRP2* and *PCDH15* expression levels. Overexpression of miR-22-3p or miR-22-5p mimics in GBM cells resulted in a decrease in SFRP2 or PCDH15 protein and mRNA levels, respectively (Fig. 6D and E). To assess if there was a direct interaction between the miRs and mRNAs, we used a 3′ UTR luciferase reporter assay where the luciferase mRNA is regulated by the miR binding sequence (Fig. 6F). Luciferase activity decreased by ∼50% in the

Figure 5 Continued
tumoursphere formation assays and graphic representation of quantification in miR rescue experiments. GSCs, GBM#P3 and GBM#BG7, were transfected with si-Ctrl, si-MIR22HG, siMIR22HG + miR-22-3p, or siMIR22HG + miR-22-5p. **(G)** Western blot for protein levels of Wnt/β-catenin indicators in lysates (20 μg) prepared from U87MG and GBM#P3 cells transfected with si-Ctrl, si-MIR22HG, siMIR22HG + miR-22-3p, or siMIR22HG + miR-22-5p. GAPDH was used as a loading control. **(H)** TOP/FOP luciferase activity to assess β-catenin activity in rescue experiments performed with U87MG cells transfected with si-Ctrl, si-MIR22HG, siMIR22HG + miR-22-3p, or siMIR22HG + miR-22-5p. **(I)** Representative haematoxylin and eosin staining of mouse brains implanted with U87MG or GBM#P3 cells transduced with sh-Ctrl ($n = 4$), sh-MIR22HG ($n = 4$), sh-MIR22HG + miR-22-3p ($n = 4$), sh-MIR22HG + miR-22-5p ($n = 4$). Scale bar = 2 mm. Data are shown as mean ± SEM. *$P < 0.05$, **$P < 0.01$, ***$P < 0.001$.
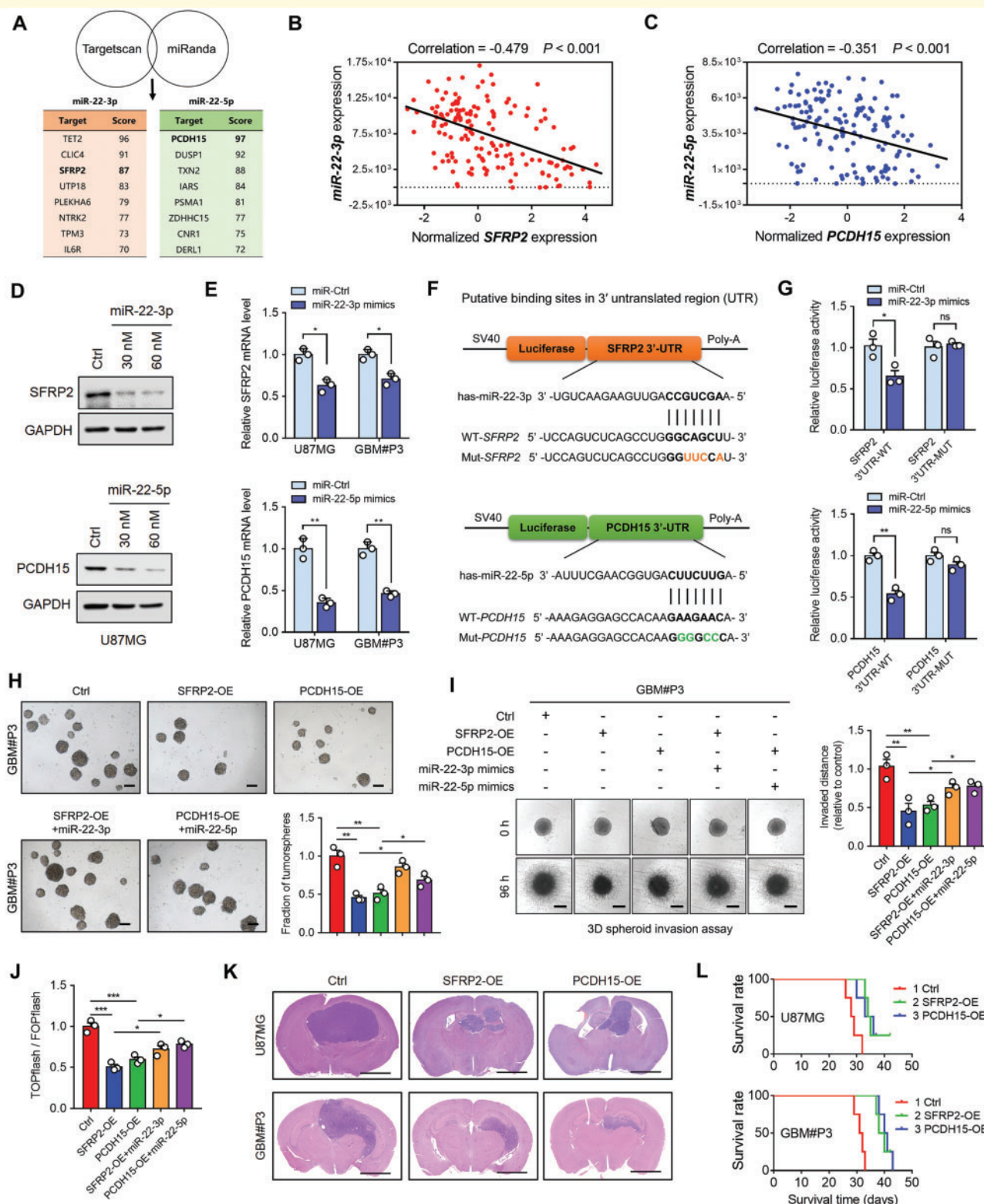
Figure 6 *SFRP2 and PCDH15 are downstream targets of miR-22 and suppress growth of GBM in vivo.* (**A**) Venn diagrams represent the candidate target genes of miR-22-3p and -5p identified by TargetScan and miRanda. (**B** and **C**) Correlation between *SFRP2* mRNA and *miR-22-3p* expression (r = −0.479, *P* < 0.001), and *PCDH15* mRNA and *miR-22-5p* expression (r = −0.351, P < 0.001) in WHO grade II–IV gliomas. (**D**) Western blot for protein levels of SFRP2 or PCDH15 from U87MG cells transfected with miR-22-3p or -5p for 48 h. GAPDH was used as a loading control. (**E**) qRT-PCR analysis for *SFRP2* or *PCDH15* mRNA levels 48 h after transfection of U87MG or GBM#P3 with miR-Ctrl, or miR-22-3p or -5p mimics. (**F**) Alignment of predicted binding sites in the *SFRP2* 3′ UTR for miR-22-3p and the *PCDH15* 3′ UTR for miR-22-5p, and the corresponding bases substituted for mutant binding sequences. Wild-type and modified UTRs are cloned into a reporter vector expressing luciferase, and luciferase activity is used to evaluate efficiency of miR targeting. (**G**) Quantitation of luciferase reporter assays in U87MG cells after

presence of the wild-type binding sequences for each of these miRs. However, mutations in the corresponding miR binding sites rendered the miR mimics ineffective in targeting the luciferase mRNA construct (Fig. 6G). In summary, these data show that SFRP2 and PCDH15 are downstream targets of miR-22.

SFRP2 and PCDH15 repress the Wnt/β-catenin pathway

We next assessed whether miR-22-3p and miR-22-5p interfered with the activity of Wnt signalling via SFRP2 or PCDH15 in GBM cells. The cells were transfected with SFRP2 or PCDH15. Overexpression was confirmed by western blots (Supplementary Fig. 10E). Ectopic expression of either SFRP2 or PCDH15 inhibited tumoursphere formation and invasion in GBM#P3 cells, which was partially reversed by co-transfection with miR-22-3p or miR-22-5p mimics, respectively (Fig. 6H and I). Consistently, transfection of miR-22-3p or miR-22-5p mimics partially rescued the suppression of β-catenin activity by SFRP2 or PCDH15, as assessed using TOP/FOP (Fig. 6J). Moreover, we observed that overexpression of SFRP2 or PCDH15 significantly blocked the miR-22-promoted tumoursphere formation in GBM#P3 cells ($P < 0.05$; Supplementary Fig. 10F). Collectively, these data suggest that miR-22-3p/SFRP2 as well as miR-22-5p/PCDH15 signalling is involved in regulating GBM development through the Wnt/β-catenin pathway. Finally, tumour growth was evaluated in a GBM orthotopic xenograft model. Overexpression of SFRP2 or PCDH15 in U87MG and GBM#P3 cells suppressed tumour growth in vivo and prolonged the overall survival of tumour-bearing mice compared to controls ($n = 4$ per group; Fig. 6K and L).

AC1L6JTK blocks the MIR22HG/miR-22 axis

Molecular docking-based virtual high-throughput screening (vHTS) is an effective in silico drug design method (Detering and Varani, 2004; Parisien and Major, 2008; Shi et al., 2013). We therefore used vHTS to identify novel compounds that might competitively combine with the Dicer binding site in the pre-miR-22 hairpin loop.

First, the 3D structure of pre-miR-22 and its hairpin loop was constructed using the MC-Fold/MC-Sym pipeline and AutoDock Vina tool (Supplementary Fig. 11A and B). Second, we performed high-throughput molecular dockings for pre-miR-22 against 4786 compounds from the National Cancer Institute (NCI) diversity set using the AutoDock Vina tool and the Lamarckian Genetic Algorithm (LGA) (Fig. 7A). Based on the virtual dockings, we discovered 50 compounds with high-binding affinity (Supplementary Table 13). Of these, NSC61610 (AC1L6JTK) had the highest affinity score (–10.7 kcal/mol; Fig. 7B) displaying half maximal inhibitory concentration (IC50) around 150 μM in GBM cells by CCK8 assay (Supplementary Fig. 11C). Based on these results, we therefore queried if AC1L6JTK could suppress the production of miR-22 in GBM cells. qRT-PCR indicated that after treatment of U87MG and GBM#P3 cells with AC1L6JTK (50 and 100 μM) for 24 h, the expression levels of both miR-22-3p and -5p were significantly decreased ($P < 0.001$, Fig. 7C).

In functional assays, the frequency of sphere formation was decreased (Fig. 7D and Supplementary Fig. 11D and E) whereas cell apoptosis was conversely increased following AC1L6JTK treatment for 48 h (Fig. 7E). AC1L6JTK treatment also attenuated transcriptional activity of β-catenin in GBM#P3 cells, similar to MIR22HG knockdown, implicating the Wnt signalling pathway as a potential target (Fig. 7F).

To assess the selectivity and specificity of AC1L6JTK interruption miR-22 generation, we analysed the effect of AC1L6JTK on seven unrelated miRNAs: miR-23a-3p, miR-155-3p, miR-720, miR-876-3p, miR-149-5p, miR-612 and miR-24-3p. After 24 h of treatment, qRT-PCR showed that the expression levels of most miRNAs were unchanged in U87MG cells, except a decrease of miR-149-5p ($P = 0.048$; Supplementary Fig. 11F). In a rescue study, AC1L6JTK treatment (100 μM) for 48 h led to an inhibition of cell growth, while this effect was restored when U87MG cells were transfected with miR-22-3p ($P < 0.01$) or miR-22-5p mimics ($P < 0.05$; Supplementary Fig. 11G). Moreover, transfection with miR-149-5p mimics could not rescue the inhibitory effect of AC1L6JTK ($P > 0.05$), indicating that

Figure 6 Continued
co-transfection of wild-type or mutated 3′ UTR luciferase constructs with the indicated miR-22 mimics (miR-Ctrl, miR-22-3p or miR-22-5p). **(H)** Representative images of tumoursphere formation assays in GBM#P3 cells transfected with expression plasmids for SFRP2 and PCDH15 (Ctrl, SFRP2-OE, or PCDH15-OE) and miR mimics (miR-22-3p or miR-22-5p). Graphic representation of the fraction of formation under the different conditions. Scale bar = 100 μm. **(I)** Representative images of 3D invasion assay and quantification in miR rescue experiments. GBM#P3 GSCs were transfected with expression plasmids for SFRP2 and PCDH15 (Ctrl, SFRP2-OE, or PCDH15-OE) and miR mimics (miR-22-3p or miR-22-5p). Scale bar = 200 μm. **(J)** TOP/FOP luciferase activity to assess β-catenin activity in rescue experiments performed in U87MG transfected with Ctrl, SFRP2-OE, or PCDH15-OE and miR-22-3p or miR-22-5p. **(K and L)** Representative haematoxylin and eosin staining of mouse brains implanted with U87MG or GBM#P3 cells expressing Ctrl ($n = 4$), SFRP2-OE ($n = 4$) or PCDH15-OE ($n = 4$), and Kaplan-Meier analysis of corresponding tumour-bearing animals. Scale bar = 2 mm. P-values were obtained from the log-rank test. Data are shown as mean ± SEM. *$P < 0.05$, **$P < 0.01$, ***$P < 0.001$.
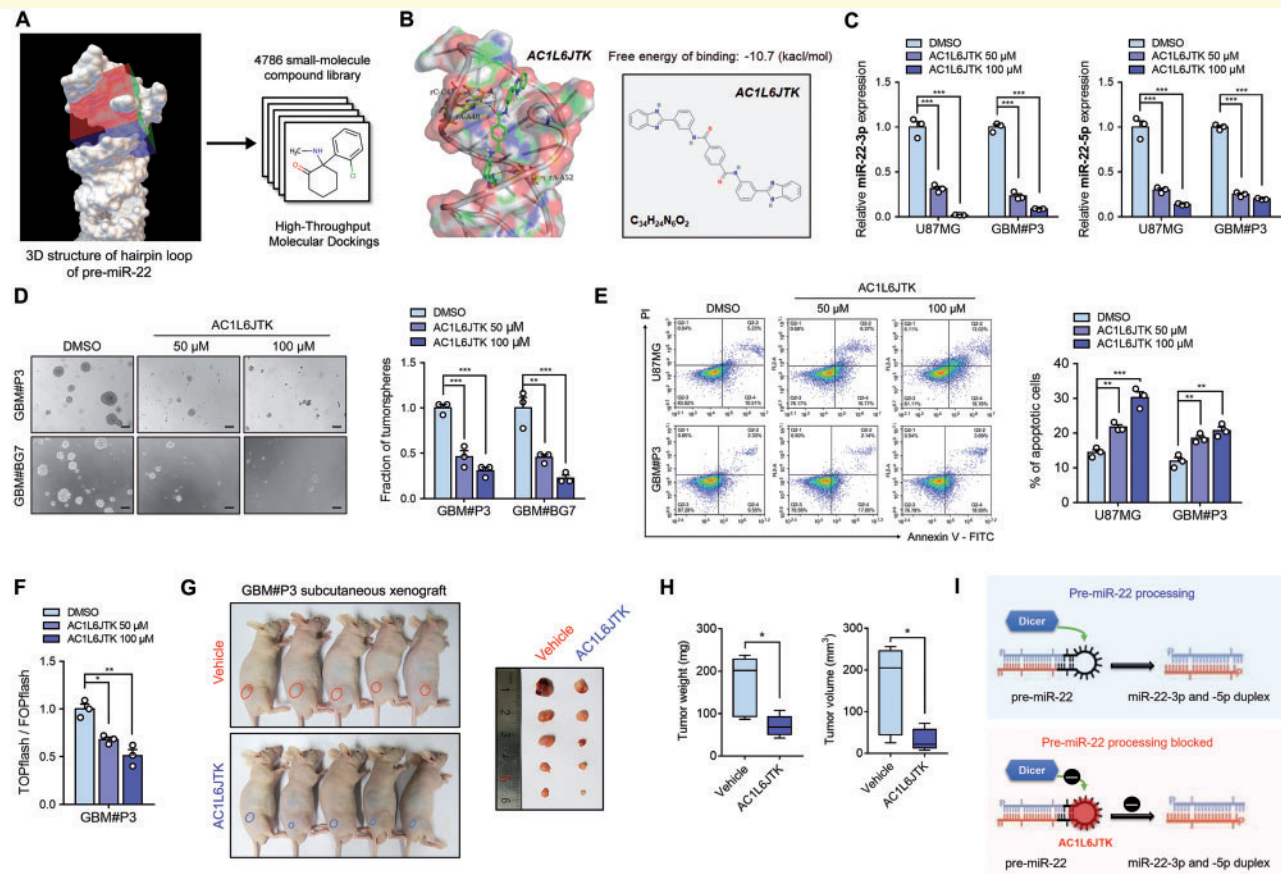
Figure 7 AC1L6JTK blocks the *MIR22HG*/miR-22 axis in GBM. (A) Schematic representation of the 3D structure of the Dicer binding site on pre-miR-22 for high-throughput molecular dockings. **(B)** Schematic representation of AC1L6JTK docking with the pre-miR-22 hairpin loop. Grid box centre is indicated by the grid boxes fixed around the Dicer-binding site. Three ribonucleotides (C47, A48 and A52) could form hydrogen bonds with AC1KL6JTK molecule structure. **(C)** qRT-PCR analysis of miR-22-3p and -5p expression in U87MG and GBM#P3 cells after AC1L6JTK (50 and 100 μM) treatment for 24 h. **(D)** Representative images from tumoursphere formation assays from GBM#P3 and GBM#BG7 after AC1L6JTK (50 and 100 μM) treatment. Scale bar = 100 μm. **(E)** Annexin V-FITC and PI staining to assess apoptosis using flow cytometry in U87MG and GBM#P3 after AC1L6JTK (50 and 100 μM) treatment. **(F)** TOP/FOP luciferase activity in GBM#P3 cells after AC1L6JTK treatment (50 and 100 μM) for 48 h. **(G** and **H)** AC1L6JTK (10 mg/kg/d) or vehicle was intraperitoneally injected into mice (*n* = 5 per group) after subcutaneous implantation of GBM#P3 cells. Tumour volumes and weights were measured from sacrificed mice (min to max box and whisker plots). **(I)** Schematic model of the inhibition of miR-22 maturation process by AC1L6JTK binding at the pre-miR-22 hairpin loop. Data are shown as mean ± SEM. *$P < 0.05$, **$P < 0.01$, ***$P < 0.001$.

miR-149-5p might not mediate *MIR22HG*-induced GBM progression.

Based on the docking results (Fig. 7B and Supplementary Fig. 12A and B), we observed three ribonucleotides in the binding pocket, C47, A48 and A52, which could form hydrogen bonds with the AC1KL6JTK molecular structure, thus competing with Dicer to inhibit *MIR22HG* processing. Consequently, to verify the specificity of AC1KL6JTK to the hairpin loop region of pre-miR-22 RNA sequence, we constructed new 3D structures of pre-miR-22 hairpin loop with point mutations at these binding sites, including MUT-1 (A52G), MUT-2 (C47T), MUT-3 (A48C) and MUT-4 (A52G, C47T, A48C) (Supplementary Fig. 12C). When AC1KL6JTK docked with these mutant 3D structures as well as the wild-type structure, the estimated free energy of binding was –7.5 kcal/mol, –8.3 kcal/mol, –7.9

kcal/mol and –7.2 kcal/mol, which were much weaker compared to the binding affinity with wild-type structure (–10.7 kcal/mol) (Supplementary Fig. 12D). These results strongly suggest that point mutations within the pre-miR-22 hairpin loop region attenuates AC1KL6JTK binding affinity and thus weaken its activity.

Molinspiration Cheminformatics software (http://www.molinspiration.com) predicted that AC1L6JTK might not efficiently penetrate the blood–brain barrier. Therefore, we evaluated the *in vivo* therapeutic efficacy of AC1L6JTK using a subcutaneous xenograft model. GBM#P3 tumours were established in nude mice, which were then randomized into either vehicle or AC1L6JTK (10 mg/kg/d) treatment groups, with drug or vehicle (DMSO) given via intraperitoneal injection. Treatment with AC1L6JTK led to a significant reduction in tumour size and

tumour weight at the treatment endpoint (Fig. 7G and 7H). These results were consistent with our *in vitro* observations.

In summary, the AC1L6JTK treatment shows that *MIR22HG* is druggable, which implies therapeutic development towards this target should be further exploited (Fig. 7I).

Discussion

LncRNAs have been linked to multiple physiological and pathological functions. More recently, studies have shown that lncRNAs are important in cancer initiation and progression (Xi *et al.*, 2018) and represent therefore potential biomarkers or therapeutic targets. However, only a small proportion of lncRNAs have been well characterized, especially in human gliomas. Here, we analysed genomic datasets from glioma patients and identified *MIR22HG* as one of the most significantly upregulated lncRNAs in GBM. We show that *MIR22HG* overexpression is associated with poor prognosis and represents a novel driver of cell proliferation and invasion. Intriguingly, we found that *MIR22HG* triggers GBM progression by producing miR-22-3p and -5p, which are encoded in exon 2 of the gene (Li *et al.*, 2010; Wang *et al.*, 2012). Finally, knockdown of *MIR22HG* in an *in vivo* orthotopic human xenograft model led to improved survival. Our results indicate that *MIR22HG* is a GBM promoting lncRNA that might serve as a novel prognostic marker in glioma patients.

MIR22HG has been reported to be involved in the development of several cancer types (Li *et al.*, 2016; Su *et al.*, 2018). Furthermore, increased expression of *MIR22HG* was observed in omental metastases when compared to matched primary ovarian tumours. Functional studies have shown that *MIR22HG* knockdown represses migration, invasion and proliferation of ovarian cancer cells (Li *et al.*, 2016). Conversely, *MIR22HG* has recently been described to mediate a tumour-suppressive effect in lung cancer and hepatocellular carcinoma (Su *et al.*, 2018; Zhang *et al.*, 2018). It has been reported that *MIR22HG* can serve as a competing endogenous RNA (ceRNA) to modulate the miRNA-10a-5p level and its downstream target gene, NCOR2, in hepatocellular carcinoma (Wu *et al.*, 2019). This discrepancy may indicate that the function of *MIR22HG* varies between different malignancies.

Dysregulation of miRNAs also contributes to malignant progression, including GBM (Banelli *et al.*, 2017). As previously reported, miR-22 has a multifaceted role during initiation and progression of various cancer types, including cell growth, cell cycle, epithelial to mesenchymal transition (EMT) and migration (Wang *et al.*, 2017). For instance, miR-22 was identified as a potent proto-oncogenic miRNA promoting proliferation and invasion of prostate cancer (Budd *et al.*, 2015). In a Cre-based mammary gland-specific transgenic mouse model, it has been demonstrated that miR-22 triggers EMT, enhances stemness, and

promotes breast cancer development and metastasis (Song *et al.*, 2013b). In haematopoietic malignancies, miR-22 enhances the repopulating capacity of haematopoietic stem progenitor cells *in vivo*, and miR-22 transgenic mice develop primary haematological diseases (Song *et al.*, 2013a). Recently, miR-22-3p was observed to be upregulated in spinal diffuse astrocytoma where it promotes glioma invasion by downregulating TIMP2, which leads to MMP2 activation (Ohnishi *et al.*, 2017). In contrast, miR-22 has also been reported to have tumour suppressive roles in some cancers. For instance, in colorectal and gastric cancers, overexpression of miR-22 significantly inhibits distant cancer metastasis by directly targeting MMP14 and Snail (Zuo *et al.*, 2015). These contradictory results underline a complex role of miR-22 function in different cancer types. In our study, both miR-22-3p and -5p were found to be highly expressed in GBM, where their expression was associated with poor clinical outcomes. Suppression of miR-22-3p and -5p by anti-miRs led to inhibition of tumour cell invasion and stemness, along with an induction of apoptosis and cell cycle arrest. In our 'rescue' experiments, the miR-22 mimics partially restored these effects in the context of *MIR22HG* knockdown *in vitro* and *in vivo*. Notably, we found that overexpression of wild-type *MIR22HG* promoted cell proliferation, while mutant *MIR22HG* (deletion of miR-22 region in exon 2) lost the growth promoting effect. Collectively, our findings indicate that miR-22-3p and -5p mediate the pro-oncogenic functions of *MIR22HG* in GBM.

Based on pathway enrichment analysis, Wnt/β-catenin signalling was one of the top 10 pathways enriched in the *MIR22HG*/miR-22 associated gene signatures. Importantly, constitutive Wnt/β-catenin activation has been observed in GBM and is essential for GBM growth, invasion and stemness (Lee *et al.*, 2016). Our results *in vitro* were consistent with the *in silico* analysis. Downregulation of *MIR22HG* led to a suppression of β-catenin transcriptional activity and thus a reduced expression of Wnt/β-catenin pathway target genes.

We also show that two genes, *SFRP2* and *PCDH15*, are direct targets of miR-22-3p and -5p inhibiting Wnt signalling in GBM. Multiple negative regulators, through various mechanisms, are natural antagonists to Wnt/β-catenin signalling. For instance, SFRPs and the Wnt inhibitory factor-1 (WIF-1) can directly bind Wnt proteins. GSK3β, however, negatively regulates the Wnt/β-catenin pathway by directly phosphorylating β-catenin, which tags it for proteasome degradation (Kogan *et al.*, 2012). SFRP2 is an antagonist of the Wnt pathway by competing for Wnt binding to Frizzled (Kawano and Kypta, 2003). However, SFRP2 also acts as an agonist of the Wnt pathway (Mirotsou *et al.*, 2007; Gehmert *et al.*, 2008; Courtwright *et al.*, 2009). In addition to the inhibition of SFRP2 by miR22 described here, SFRP2 is also downregulated in GBM via promoter hypermethylation (Kongkham *et al.*, 2010). Besides, several SFRP family members (SFRP1, 2 and 3) have been found to function as tumour suppressors in

medulloblastoma (Kongkham *et al.*, 2010). In the current study, we found that expression levels of *SFRP2* were significantly downregulated in GBM as compared to LGG and normal brain tissue. Lower expression levels of *SFRP2* were also observed in non-GSCs compared to GSCs. In functional assays, ectopic expression of SFRP2 suppressed GBM malignant behaviours and Wnt signalling activity, thus demonstrating its tumour-suppressive role in GBM.

Protocadherins play important roles in the regulation of cell adhesion and signal transduction. Recently, multiple members of the protocadherin family were found to suppress tumour progression by antagonizing the Wnt/β-catenin pathway (Mah and Weiner, 2017). Although PCDH15 suppression of this pathway has not been previously demonstrated, we found in GSCs that ectopic expression of PCDH15 led to a significant reduction of sphere formation and invasion. This coincided with a decrease in Wnt activity. The inhibitory effect was partially restored by co-transfection of miR-22-5p (or miR-22-3p in the case of *SFRP2*) mimics. Although we found that miR-22-3p and miR-22-5p work together to target negative regulators of Wnt signalling, providing a previously unknown regulatory mechanism of this pathway, we cannot exclude the possibility that these microRNAs contribute to glioma progression through other mechanisms than Wnt signalling.

Exact knowledge on how *MIR22HG* is processed into miRs can be used for pharmacological interference based on Dicer, an enzyme that is essential for cleavage of the terminal hairpin loop of precursor microRNAs (pre-miRNAs) to produce mature miRNAs. Based on the 3D structure of pre-miR-22 and its hairpin loop (the Dicer binding site), we performed high-throughput molecular dockings for pre-miR-22 against the 4786 compounds using the NCI diversity set. We identified a small-molecule inhibitor of *MIR22HG*/miR-22, AC1L6JTK, which efficiently suppressed the expression of miR-22-3p and -5p in GBM cells. Interestingly, AC1L6JTK has previously been tested for therapeutic efficacy in inflammatory bowel disease (Lu *et al.*, 2012, 2014). In the present study, we found that AC1L6JTK treatment inhibited GBM proliferation and induced apoptosis, indicating that AC1L6JTK could be used as an anticancer agent in GBM (see schematic representation Supplementary Fig. 11). However, the molecule requires further optimization in particular with regard to blood–brain barrier penetration.

In conclusion, our work not only uncovers an oncogenic role for *MIR22HG* in promoting GBM aggressiveness and GSC self-renewal, but also implicates *MIR22HG*/miR-22 as a potential target for treating gliomas through pharmacological blockade.

Acknowledgements

Funding

Competing interests

The authors report no competing interests.

Supplementary material

Supplementary material is available at *Brain* online.

References

Adams BD, Parsons C, Walker L, Zhang WC, Slack FJ. Targeting noncoding RNAs in disease. J Clin Invest 2017; 127: 761–71.

Alvarado AG, Turaga SM, Sathyan P, Mulkearns-Hubert EE, Otvos B, Silver DJ, et al. Coordination of self-renewal in glioblastoma by integration of adhesion and microRNA signaling. Neuro Oncol 2016; 18: 656–66.

Banelli B, Forlani A, Allemanni G, Morabito A, Pistillo MP, Romani M. MicroRNA in glioblastoma: an overview. Int J Genomics 2017; 2017: 7639084.

Bjerkvig R, Laerum OD, Mella O. Glioma cell interactions with fetal rat brain aggregates in vitro and with brain tissue in vivo. Cancer Res 1986; 46: 4071–9.

Budd WT, Seashols-Williams SJ, Clark GC, Weaver D, Calvert V, Petricoin E, et al. Dual action of miR-125b as a tumor suppressor and OncomiR-22 promotes prostate cancer tumorigenesis. PLoS One 2015; 10: e0142373.

Ceccarelli M, Barthel FP, Malta TM, Sabedot TS, Salama SR, Murray BA, et al. Molecular profiling reveals biologically discrete subsets and pathways of progression in diffuse glioma. Cell 2016; 164: 550–63.

Cech TR, Steitz JA. The noncoding RNA revolution-trashing old rules to forge new ones. Cell 2014; 157: 77–94.

Chen Q, Cai J, Wang Q, Wang Y, Liu M, Yang J, et al. Long noncoding RNA NEAT1, regulated by the EGFR pathway, contributes to glioblastoma progression through the WNT/beta-catenin pathway by scaffolding EZH2. Clin Cancer Res 2018; 24: 684–95.

Chen ZH, Hu HK, Zhang CR, Lu CY, Bao Y, Cai Z, et al. Downregulation of long non-coding RNA FOXD3 antisense RNA 1 (FOXD3-AS1) inhibits cell proliferation, migration, and invasion in malignant glioma cells. Am J Transl Res 2016; 8: 4106–19.

Courtwright A, Siamakpour-Reihani S, Arbiser JL, Banet N, Hilliard E, Fried L, et al. Secreted frizzle-related protein 2 stimulates angiogenesis via a calcineurin/NFAT signaling pathway. Cancer Res 2009; 69: 4621–8.

Detering C, Varani G. Validation of automated docking programs for docking and database screening against RNA drug targets. J Med Chem 2004; 47: 4188–201.

Fack F, Espedal H, Keunen O, Golebiewska A, Obad N, Harter PN, et al. Bevacizumab treatment induces metabolic adaptation toward anaerobic metabolism in glioblastomas. Acta Neuropathol 2015; 129: 115–31.

Gehmert S, Sadat S, Song YH, Yan Y, Alt E. The anti-apoptotic effect of IGF-1 on tissue resident stem cells is mediated via PI3-kinase dependent secreted frizzled related protein 2 (Sfrp2) release. Biochem Biophys Res Commun 2008; 371: 752–5.

Gupta RA, Shah N, Wang KC, Kim J, Horlings HM, Wong DJ, et al. Long non-coding RNA HOTAIR reprograms chromatin state to promote cancer metastasis. Nature 2010; 464: 1071–6.

Hacisuleyman E, Goff LA, Trapnell C, Williams A, Henao-Mejia J, Sun L, et al. Topological organization of multichromosomal regions by the long intergenic noncoding RNA Firre. Nat Struct Mol Biol 2014; 21: 198–206.

Hui J, Zhang J, Pu M, Zhou X, Dong L, Mao X, et al. Modulation of GSK-3beta/beta-Catenin Signaling Contributes to Learning and Memory Impairment in a Rat Model of Depression. Int J Neuropsychopharmacol 2018; 21: 858–70.

Jiang T, Mao Y, Ma W, Mao Q, You Y, Yang X, et al. CGCG clinical practice guidelines for the management of adult diffuse gliomas. Cancer Lett 2016; 375: 263–73.

Joseph JV, Conroy S, Tomar T, Eggens-Meijer E, Bhat K, Copray S, et al. TGF-beta is an inducer of ZEB1-dependent mesenchymal transdifferentiation in glioblastoma that is associated with tumor invasion. Cell Death Dis 2014; 5: e1443.

Kawano Y, Kypta R. Secreted antagonists of the Wnt signalling pathway. J Cell Sci 2003; 116: 2627–34.

Kogan Y, Halevi-Tobias KE, Hochman G, Baczmanska AK, Leyns L, Agur Z. A new validated mathematical model of the Wnt signalling pathway predicts effective combinational therapy by sFRP and Dkk. Biochem J 2012; 444: 115–25.

Kongkham PN, Northcott PA, Croul SE, Smith CA, Taylor MD, Rutka JT. The SFRP family of WNT inhibitors function as novel tumor suppressor genes epigenetically silenced in medulloblastoma. Oncogene 2010; 29: 3017–24.

Lee Y, Lee JK, Ahn SH, Lee J, Nam DH. WNT signaling in glioblastoma and therapeutic opportunities. Lab Invest 2016; 96: 137–50.

Li J, Yu H, Xi M, Lu X. Long noncoding RNA C17orf91 is a potential prognostic marker and functions as an oncogene in ovarian cancer. J Ovarian Res 2016; 9: 49.

Li VS, Ng SS, Boersema PJ, Low TY, Karthaus WR, Gerlach JP, et al. Wnt signaling through inhibition of beta-catenin degradation in an intact Axin1 complex. Cell 2012; 149: 1245–56.

Li X, Liu J, Zhou R, Huang S, Huang S, Chen XM. Gene silencing of MIR22 in acute lymphoblastic leukaemia involves histone modifications independent of promoter DNA methylation. Br J Haematol 2010; 148: 69–79.

Liu S, Yin F, Zhang J, Wicha MS, Chang AE, Fan W, et al. Regulatory roles of miRNA in the human neural stem cell transformation to glioma stem cells. J Cell Biochem 2014; 115: 1368–80.

Louis DN, Perry A, Reifenberger G, von Deimling A, Figarella-Branger D, Cavenee WK, et al. The 2016 World Health Organization classification of tumors of the central nervous system: a summary. Acta Neuropathol 2016; 131: 803–20.

Lu P, Hontecillas R, Horne WT, Carbo A, Viladomiu M, Pedragosa M, et al. Computational modeling-based discovery of novel classes of anti-inflammatory drugs that target lanthionine synthetase C-like protein 2. PLoS One 2012; 7: e34643.

Lu P, Hontecillas R, Philipson CW, Bassaganya-Riera J. Lanthionine synthetase component C-like protein 2: a new drug target for inflammatory diseases and diabetes. Curr Drug Targets 2014; 15: 565–72.

Mah KM, Weiner JA. Regulation of Wnt signaling by protocadherins. Semin Cell Dev Biol 2017; 69: 158–71.

Malik R, Patel L, Prensner JR, Shi Y, Iyer MK, Subramaniyan S, et al. The lncRNA PCAT29 inhibits oncogenic phenotypes in prostate cancer. Mol Cancer Res 2014; 12: 1081–7.

Mirotsou M, Zhang Z, Deb A, Zhang L, Gnecchi M, Noiseux N, et al. Secreted frizzled related protein 2 (Sfrp2) is the key Akt-mesenchymal stem cell-released paracrine factor mediating myocardial survival and repair. Proc Natl Acad Sci USA 2007; 104: 1643–8.

Ohnishi YI, Iwatsuki K, Ishihara M, Ohkawa T, Kinoshita M, Shinzawa K, et al. Promotion of astrocytoma cell invasion by micro RNA-22 targeting of tissue inhibitor of matrix metalloproteinase-2. J Neurosurg Spine 2017; 26: 396–403.

Parisien M, Major F. The MC-Fold and MC-Sym pipeline infers RNA structure from sequence data. Nature 2008; 452: 51–5.

Paul Y, Thomas S, Patil V, Kumar N, Mondal B, Hegde AS, et al. Genetic landscape of long noncoding RNA (lncRNAs) in glioblastoma: identification of complex lncRNA regulatory networks and clinically relevant lncRNAs in glioblastoma. Oncotarget 2018; 9: 29548–64.

Pollard SM, Yoshikawa K, Clarke ID, Danovi D, Stricker S, Russell R, et al. Glioma stem cell lines expanded in adherent culture have tumor-specific phenotypes and are suitable for chemical and genetic screens. Cell Stem Cell 2009; 4: 568–80.

Puchalski RB, Shah N, Miller J, Dalley R, Nomura SR, Yoon JG, et al. An anatomic transcriptional atlas of human glioblastoma. Science 2018; 360: 660–3.

Reon BJ, Anaya J, Zhang Y, Mandell J, Purow B, Abounader R, et al. Expression of lncRNAs in Low-Grade Gliomas and Glioblastoma Multiforme: an In Silico Analysis. PLoS Med 2016; 13: e1002192.

Sahu A, Singhal U, Chinnaiyan AM. Long noncoding RNAs in cancer: from function to translation. Trends Cancer 2015; 1: 93–109.

Shi Z, Zhang J, Qian X, Han L, Zhang K, Chen L, et al. AC1MMYR2, an inhibitor of dicer-mediated biogenesis of Oncomir miR-21, reverses epithelial-mesenchymal transition and suppresses tumor growth and progression. Cancer Res 2013; 73: 5519–31.

Song SJ, Ito K, Ala U, Kats L, Webster K, Sun SM, et al. The oncogenic microRNA miR-22 targets the TET2 tumor suppressor to promote hematopoietic stem cell self-renewal and transformation. Cell Stem Cell 2013a; 13: 87–101.

Song SJ, Poliseno L, Song MS, Ala U, Webster K, Ng C, et al. MicroRNA-antagonism regulates breast cancer stemness and metastasis via TET-family-dependent chromatin remodeling. Cell 2013b; 154: 311–24.

Su W, Feng S, Chen X, Yang X, Mao R, Guo C, et al. Silencing of long noncoding RNA MIR22HG triggers cell survival/death signaling via oncogenes YBX1, MET, and p21 in lung cancer. Cancer Res 2018; 78: 3207–19.

Trimarchi T, Bilal E, Ntziachristos P, Fabbri G, Dalla-Favera R, Tsirigos A, et al. Genome-wide mapping and characterization of Notch-regulated long noncoding RNAs in acute leukemia. Cell 2014; 158: 593–606.

Wang J, Li Y, Ding M, Zhang H, Xu X, Tang J. Molecular mechanisms and clinical applications of miR-22 in regulating malignant progression in human cancer (Review). Int J Oncol 2017; 50: 345–55.

Wang J, Xiang G, Zhang K, Zhou Y. Expression signatures of intragenic miRNAs and their corresponding host genes in myeloid leukemia cells. Biotechnol Lett 2012; 34: 2007–15.

Wang X, Prager BC, Wu Q, Kim LJY, Gimple RC, Shi Y, et al. Reciprocal signaling between glioblastoma stem cells and differentiated tumor cells promotes malignant progression. Cell Stem Cell 2018; 22: 514–28.e5.

Wu X, Wang Y, Yu T, Nie E, Hu Q, Wu W, et al. Blocking MIR155HG/miR-155 axis inhibits mesenchymal transition in glioma. NeuroOncol 2017; 19: 1195–205.

Wu Y, Zhou Y, Huan L, Xu L, Shen M, Huang S, et al. LncRNA MIR22HG inhibits growth, migration and invasion through regulating the miR-10a-5p/NCOR2 axis in hepatocellular carcinoma cells. Cancer Sci 2019; 110: 973–84.

Xi J, Sun Q, Ma L, Kang J. Long non-coding RNAs in glioma progression. Cancer Lett 2018; 419: 203–9.

Yan H, Parsons DW, Jin G, McLendon R, Rasheed BA, Yuan W, et al. IDH1 and IDH2 mutations in gliomas. N Engl J Med 2009; 360: 765–73.

Yoon JH, Abdelmohsen K, Srikantan S, Yang X, Martindale JL, De S, et al. LincRNA-p21 suppresses target mRNA translation. Mol Cell 2012; 47: 648–55.

Yuan JH, Yang F, Wang F, Ma JZ, Guo YJ, Tao QF, et al. A long noncoding RNA activated by TGF-beta promotes the invasion-metastasis cascade in hepatocellular carcinoma. Cancer Cell 2014; 25: 666–81.

Zhang DY, Zou XJ, Cao CH, Zhang T, Lei L, Qi XL, et al. Identification and functional characterization of long non-coding RNA MIR22HG as a tumor suppressor for hepatocellular carcinoma. Theranostics 2018; 8: 3751–65.

Zhang JX, Han L, Bao ZS, Wang YY, Chen LY, Yan W, et al. HOTAIR, a cell cycle-associated long noncoding RNA and a strong predictor of survival, is preferentially expressed in classical and mesenchymal glioma. NeuroOncol 2013; 15: 1595–603.

Zhang K, Sun X, Zhou X, Han L, Chen L, Shi Z, et al. Long non-coding RNA HOTAIR promotes glioblastoma cell cycle progression in an EZH2 dependent manner. Oncotarget 2015; 6: 537–46.

Zheng J, Liu X, Wang P, Xue Y, Ma J, Qu C, et al. CRNDE promotes malignant progression of glioma by attenuating miR-384/PIWIL4/ STAT3 Axis. Mol Ther 2016; 24: 1199–215.

Zhou K, Zhang C, Yao H, Zhang X, Zhou Y, Che Y, et al. Knockdown of long non-coding RNA NEAT1 inhibits glioma cell migration and invasion via modulation of SOX2 targeted by miR-132. Mol Cancer 2018; 17: 105.

Zuo QF, Cao LY, Yu T, Gong L, Wang LN, Zhao YL, et al. MicroRNA-22 inhibits tumor growth and metastasis in gastric cancer by directly targeting MMP14 and Snail. Cell Death Dis 2015; 6: e2000.